Featured in Physics

Photonic Flatband Resonances in Multiple Light Scattering

Thanh Xuan Hoang,[1] Daniel Leykam,[2] and Yuri Kivshar[3]

[1]*Institute of High Performance Computing (IHPC), Agency for Science, Technology and Research (A*STAR), 1 Fusionopolis Way, #16-16 Connexis, Singapore 138632, Republic of Singapore*

[2]*Centre for Quantum Technologies, National University of Singapore, 3 Science Drive 2, Singapore 117543, Singapore*

[3]*Nonlinear Physics Center, Research School of Physics, Australian National University, Canberra ACT 2601, Australia*

(Received 1 June 2023; accepted 7 December 2023; published 23 January 2024)

We introduce the concept of photonic flatband resonances and demonstrate it for an array of high-index dielectric particles. We employ the multiple Mie scattering theory and demonstrate that both short- and long-range interactions between the resonators are crucial for the emerging *collective resonances* and their associated *photonic flatbands*. By examining both near- and far-field characteristics, we uncover how the flatbands emerge due to a fine tuning of resonators' radiation fields, and predict that hybridization of a flatband resonance with an electric hot spot can lead to giant values of the Purcell factor for the electric dipolar emitters.

DOI: 10.1103/PhysRevLett.132.043803

Introduction.—The physics of the systems with flatband spectra (or flatbands) has attracted a lot of attention recently, in connection with the studies of electronic periodic structures with nontrivial topology [1,2]. One of the important features of the flatband systems is that their density of states grows with the system size, in contrast to regular lattices where the density of states generally remains finite. The enhanced density of states in flatbands allows one to achieve strong interaction in electronic systems [3,4] and photonics [5,6], with applications to quantum networks [7,8], on-chip single-photon generation [9] and nanolasers [10], as well as compact free-electron light sources [11].

Importantly, a majority of the previous studies of flatbands involved the systems with engineered symmetries and couplings that are short-ranged either in real space [12] or Fourier space [13], being described by the tight-binding models or coupled-mode theories. However, recent demonstrations of electronic and photonic moiré superlattices revealed that the flatbands may emerge from parameter fine-tuning in more general settings involving interactions between many states in lattices with complex unit cells [14–21]. While the physics of flatbands remains an open question beyond the short-range coupling approximation, minimal effective tight-binding models developed for magic angle bilayer graphene suggest that fine-tuned coupling between strongly and weakly localized states may play an important role [22,23], in contrast to short-range interaction that typically destroys the flatbands.

We notice that couplings between states of very different nature occur routinely in photonics; while electronic systems described by the Schrödinger equation support localized negative energy bound states, light waves always have a positive energy and thus generally couple to radiation channels supported by the surrounding environment. Multipole-based models offer a powerful approach for faithfully describing couplings between localized and radiation states [24–27], taking into account the anisotropy of near-field scattering, coupling and interference between different scattering multipole orders, and all the radiation channels in the surrounding three-dimensional (3D) environment. However, these effects are expected to spoil the fine-tuned wave interference leading to flatbands in simpler effective models.

In this Letter, we employ the multipole Mie scattering to demonstrate the emergence of photonic flatbands due to fine-tuning of interaction in a simple one-dimensional (1D) chain of high-index dielectric nanoparticles. Multiple scattering theory (MST) plays a crucial role in many fundamental wave phenomena, such as the Anderson localization of electrons and light [28]. The MST approach allows one to identify flatbands emerging as exact solutions to Maxwell's equations and study how their hybridization with electronic hot spot modes can lead to giant enhancement of the Purcell factor for electronic dipolar emitters [29]. We find that coupling between different multipoles, which is typically considered in the context of short-range interactions [30–32], also has a significant role in shaping the radiative losses [29,33,34]. Most photonic flatbands have been based on fine-tuned couplings between different sublattices of resonators designed using tight-binding

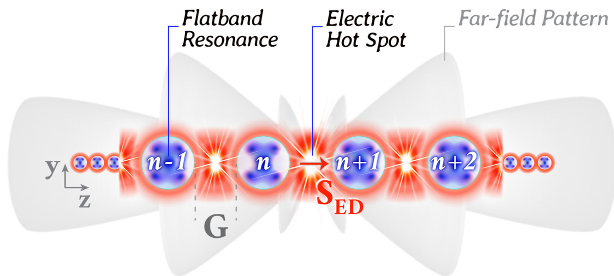

FIG. 1. Schematic of multipole Mie scattering for an electric dipole S_{ED} interacting with a chain of dielectric spheres. The flatband resonance and electric hot spot modes are inseparable from the collective resonances and their far-field patterns.

models [5]; our MST shows how flatband physics can emerge in much broader classes of resonator lattices due to competition between near- and far-field coupling.

Model.—We consider the interaction between a z-oriented electric dipolar emitter S_{ED} with dipole moment μ and a linear chain of identical silicon spheres with refractive index 3.5, radius 210 nm, and separation G embedded in vacuum, shown in Fig. 1. These parameters ensure the photonic modes of interest fall within the near-infrared frequency range, which is relevant for various scientific and technological applications [35]. We expand the field scattered by the uth sphere positioned at $\mathbf{r}_u$ as a series of electric multipole fields $\mathbf{N}_{l;m}$ [29,36]

$$\mathbf{E}_u(\mathbf{r}) = \sum_{l=1}^{L_u} p_{l;0}^{(u)} \mathbf{N}_{l;0}(k[\mathbf{r}-\mathbf{r}_u]), \tag{1}$$

where the required truncation order L_u depends on the vacuum wave number k and the spheres' radius; here $L_u = 10$ is sufficient to obtain good agreement with a direct numerical solution of Maxwell's equations (Lumerical FDTD) [37]. Note that due to the axial symmetry the source excites only the $m = 0$ electric multipole modes.

In the multiple Mie scattering theory the interaction between the dipolar emitter and the spheres, as well as the coupling between the spheres' scattering multipole expansion coefficients (MECs) is described by

$$p_{l';0}^{(n)} = a_{l'}^{(n)} \left(A_{l';0}^{1;0}(\overrightarrow{OO_n})\mu + \sum_{u\neq n} \sum_{l=1}^{L_u} A_{l';0}^{l;0}(\overrightarrow{O_u O_n}) p_{l;0}^{(u)} \right), \tag{2}$$

where $A_{l';0}^{l;0}(\overrightarrow{O_u O_n})$ translates the multipole field of $\mathbf{N}_{l;0}$ from the uth sphere into the incident field approaching the nth sphere [29]. Equation (2) accounts for both the short-range ($u = n \pm 1$) and long-range couplings ($u \neq n \pm 1$) between the multiple scattering fields; it also includes the off-diagonal coupling between different multipolar orders, i.e., $l' \neq l$. Implicitly, Eq. (2) also accounts for the coupling between the near field and the fields of an extensive number of radiation channels supported by the 3D vacuum, since each multipole term $\mathbf{N}_{l;0}$ contributes to the far field [33].

After solving Eq. (2) to obtain the individual spheres' MECs $p_{l;0}^{(u)}$, the far field can be obtained by summing the source field and the scattering fields from the spheres and performing a multipolar expansion of order L_{tot} about the origin using the vector addition theorem [29,38,39]

$$\mathbf{E}^{\mathrm{tot}}(\mathbf{r}) = \sum_{l=1}^{L_{\mathrm{tot}}} \alpha_{l;0} \mathbf{N}_{l;0}(k\mathbf{r}), \tag{3}$$

where the eigenfunctions $\mathbf{N}_{l;0}$ represent modes of the Universe including the emitter, spheres, and their environment. The coefficients $\alpha_{l;0}$ implicitly take into account interference between the dipole source and scattered fields. The enhancement of the local density of states (LDOS) at S_{ED} provided by the modes of Eq. (3) is described by the Purcell factor

$$F_P = \frac{1}{2|\mu|^2} \sum_{l=1}^{L_{\mathrm{tot}}} l(l+1)|\alpha_{l;0}|^2, \tag{4}$$

which is given by the total power radiating into the far-field P divided by the radiating power of an isolated S_{ED} source, $P_0 = c|\mu|^2/(4\pi)$. Thus, after obtaining the field generated by a dipolar source as a function of k by solving Eq. (2), $F_P(k)$ can be computed using Eq. (4) to identify resonances associated with excitations of the collective modes of the chain of nanospheres.

Collective resonances.—Figures 2(a) and 2(b) present the near-field distributions and F_P spectrum of three collective $L_{1,2,3}$ resonances supported by a 30-sphere chain and excited by an S_{ED} source located at the center of the gap between the 7th and 8th spheres. Although the near-field distributions may appear similar to Fabry-Perot cavity modes [40,41], it is important to note that the latter are due to propagating waves and only experience radiative losses at the ends of their cavity, as observed in nanowires [10,42]. In contrast, the radiative losses of the three $L_{1,2,3}$ resonances, described by Eq. (2), occur along the entire chain, with the main contributors being the scatterings by the middle spheres [37].

Figure 2(b) demonstrates the essential role of long-range couplings in the physics of collective resonances. The exact MST model, incorporating both short- and long-range couplings as described in Eq. (2), reveals three resonant peaks around the wavelength of 1000 nm. In contrast, the blue line, representing short-range coupling alone, fails to capture the manifestation of collective resonances. Equation (2) with the omission of long-range coupling can be analogously viewed as a tight-binding model, focusing solely on interactions between neighboring spheres. Therefore, our findings may provide novel insights into the results of similar models centered on the interaction

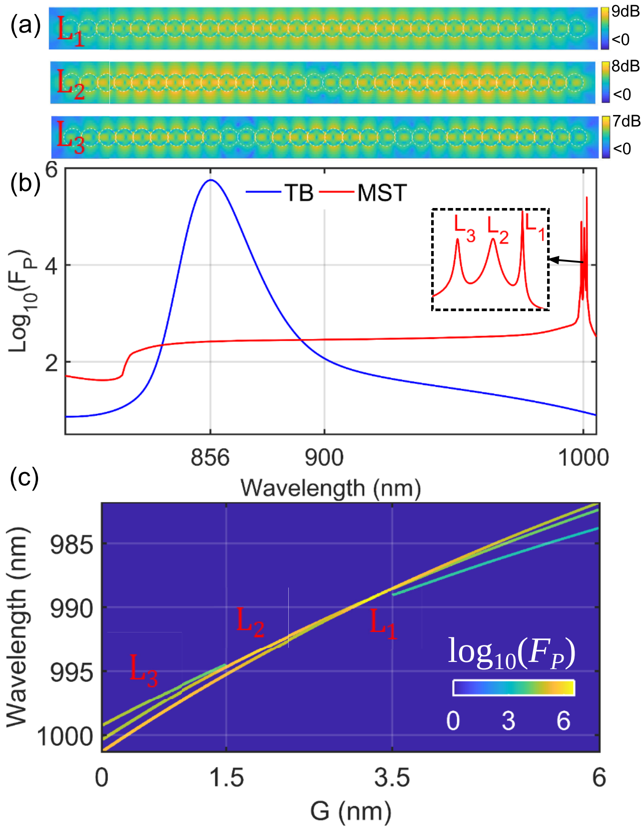

FIG. 2. Collective Mie resonances and their crossing regime. (a) Electric near-field distributions of the three collective quadrupole resonances excited by a dipolar emitter in a 30-sphere chain with the interparticle gap size $G = 0$ nm. (b) The tight-binding (TB) model, which considers short-range couplings only, fails to capture the collective resonances present in the red line of the exact multiple scattering theory (MST). (c) Crossing and disappearance of the three collective $L_{1;2;3}$ resonances from the fine-tuning of G.

of nearest-neighbor particles [40,43]. Figure 2(b) also shows the significant impact of the electric hot spot mode on the LDOS, visible as a enhancement of F_P by more than 2 orders of magnitude even for off-resonant wavelengths.

The multiple Mie scattering theory highlights the critical role played by both short- and long-range couplings in nanophotonics. Our chain extends over tens of wavelengths while maintaining a subwavelength period. As a result, the short-range coupling primarily engages near-field interactions, whereas the long-range coupling encompasses interactions in the far-field domain, including radiation losses. The interplay and competition between these near- and far-field couplings emerge as pivotal elements contributing to the formation of collective resonances. Furthermore, the off-diagonal couplings between different multipole orders are also crucial to accurately describe the LDOS enhancement [44–46].

Figure 2(c) shows the merging of the three collective resonances, visually represented through their respective peak F_P values and corresponding wavelengths when fine-tuning G. As we increase G from 0 to 1.5 nm, the chain transitions into the supercavity regime, corresponding to a crossing of the resonances; the L_3 resonance merges with and enhances the lifetime of the L_2 resonance to become even stronger than the L_1 resonance [35]. The enhancement of the L_2 resonance comes at the cost of reducing the lifetime of the L_3 resonance, completely obscuring it for $G \in (1.5, 3.5)$ nm. The L_2 resonance reaches its peak at $G = 1.8$ nm, where its F_P is sixfold higher than that of the L_1 resonance [37].

The outstanding performance of the supercavity L_2 resonance is well recognized within Feshbach's theory of overlapping resonances, which is described by a coupled-channel Schrödinger equation. When two closed channels couple to one open channel, a Friedrich-Wintgen bound state in the continuum (BIC) supported by a finite potential structure can be observed for anticrossing modes [47–49]. The supercavity L_2 resonance can be considered similar to a Friedrich-Wintgen BIC because its linewidth is much narrower at $G = 1.8$ nm ($\Delta\lambda \approx 0.012$ nm, or equivalently a quality factor of $Q \approx 8.3 \times 10^4$) than at $G = 0$ nm ($\Delta\lambda \approx 0.22$ nm, or $Q \approx 4.5 \times 10^3$). We also observe a supercavity L_1 resonance peaking at $G = 3.225$ nm with $Q \approx 1.4 \times 10^6$, where the L_2 resonance crosses into the L_1 resonance. In the supercavity regime, the multiple scattering fields of the spheres interfere destructively at distant locations while constructively enhancing at the central spheres. This phenomenon results in a remarkable near-field enhancement at the center accompanied by a merging of scattering loss channels [35,37].

In contrast to the compact Friedrich-Wintgen BICs for matter waves, which in theory have a vanishing linewidth, light waves always have a positive energy and thus practically couple to an extensive number of radiation channels supported by the surrounding 3D vacuum, leading to a nonzero linewidth ($\Delta\lambda \neq 0$ nm). The Friedrich-Wintgen BIC theory assumes that two closed channels couple to one open channel, but this assumption is not valid for photonic systems due to the presence of the extensive number of radiation channels, approximated in terms of a finite number of multipoles in multipole scattering theory [33]. Feshbach's theory shows that one can mathematically reduce open channels to one continuum; eliminating an open channel results in an effective complex potential with an imaginary part that accounts for the energy loss associated with the eliminated open channel [47]. While Feshbach-type matter BICs facilitated by complex-potential structures remain unexplored, we expect their characteristics to be similar to our supercavity modes, drawing from the analogy between matter and light waves exhibiting positive energies [28].

We present the internal field and far-field characteristics of the supercavity resonances in Fig. 3. The spheres' internal fields can be expanded as a multipole series with

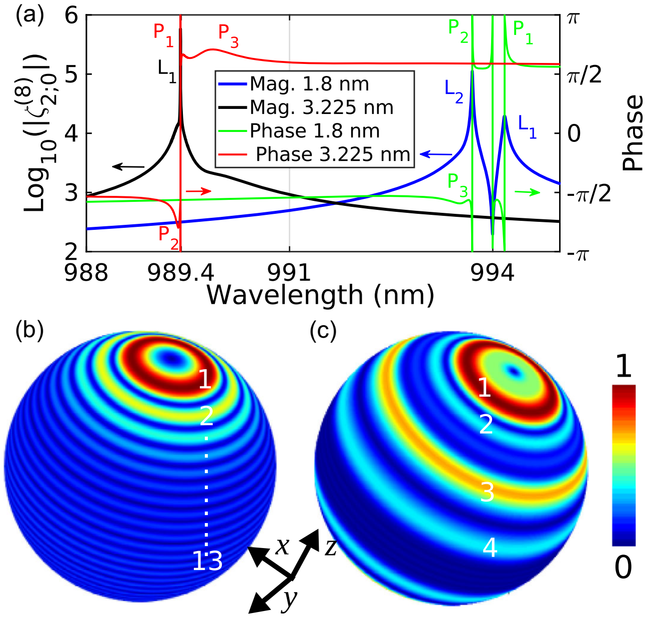

FIG. 3. (a) Magnitude and phase of the EQ coefficient $\zeta_{2;0}^{(8)}$ for the two cases of $G = 1.8$ nm and $G = 3.225$ nm. Far-field patterns of the L_1 resonance for the two cases of $G = 0$ nm (b) and $G = 3.225$ nm (c) show the merging of the scattering channels.

coefficients $\zeta_{l;0}^{(u)}$, which are related to to the scattering MECs $p_{l;0}^{(u)}$ in Eq. (1) via $\zeta_{l;0}^{(u)} = p_{l;0}^{(u)} c_l^{(u)} / a_l^{(u)}$, where $a_l^{(u)}$ and $c_l^{(u)}$ are the Mie coefficients [50]. The collective resonances are dominated by the internal electric quadrupole (EQ) coefficients.

Figure 3(a) presents the magnitude and phase of the EQ coefficient representing the internal field of the 8th sphere for the two cases of $G = 1.8$ nm and $G = 3.225$ nm. The spectral profiles of the magnitude, which agree with the F_P evolution in Fig. 2(c), show that the crossing of the two $L_{1,2}$ modes leads to the disappearance of the L_2 mode at $G = 3.225$ nm. In contrast to the magnitude plots, the phase plots always exhibit the signatures of all the three $L_{1,2,3}$ resonances. In the case of $G = 3.225$ nm, the disappearance of the L_2 resonance manifests itself as a strong phase fluctuation around the black L_1 peak, resulting in a small phase trough marked by the red P_2. This phenomenon is consistent with Feshbach's theory of two interfering resonances, where one resonance becomes sharper and the other becomes more lossy. Additionally, the phase jumps across the peaks in the spectral phase plots are not exactly π, due to coupling to other multipoles [47]. At the enhancement and suppression points, the EQ coefficient becomes real, causing the phase changes of 2π.

Figures 3(b) and 3(c) present the physics of the supercavity L_1 resonance from a far-field perspective. Without the resonance crossing ($G = 0$ nm), the collective L_1 resonance exhibits high radiative losses, as shown in Fig. 3(b), which displays 27 circular fringes. Each fringe may be understood as a separate scattering loss channel. The far-field distribution of the supercavity L_1 resonance in Fig. 3(c) shows a reduced number of only 8 scattering loss channels, giving improved light trapping efficiency compared to the normal L_1 resonance. Remarkably, this non-vanishing far field of the supercavity resonance is also a characteristic feature of Feshbach-type BICs–which include the Friedrich-Wintgen BICs–in the context of formal scattering theory [35,51].

Flatband resonance.—As the number of spheres is increased, the chain transitions into a quasi-1D photonic crystal (PC) [52–54]. Previous studies have shown that the bandwidth of this type of PC corresponds to the spectral range enclosing all the collective resonances of the same Mie modes [10,37,55]. The spectral degeneracy of the three collective $L_{1,2,3}$ resonances to form the supercavity L_1 resonance suggests that the associated PC bandwidth vanishes, resulting in a flatband. To obtain a more accurate estimation of the bandwidths of the associated PC we consider chains of up to 100 spheres [10].

Figure 4(a) shows the dependence of the supercavity L_1 resonance on the number of spheres, demonstrating the convergence of its resonant wavelength and the corresponding G toward 986 nm and 4.5 nm, respectively. This suggests that a flatband of the PC with a period of 424.5 nm will occur at a single wavelength of 986 nm, which is confirmed in Fig. 5. In finite chains, the flatband is represented by the supercavity L_1 resonance, which provides extreme enhancement of the LDOS as shown in Fig. 4(b). For comparison, the Purcell factor F_P for the case of $G = 10$ nm is also shown. The supercavity L_1 resonances provide much larger enhancement compared to the normal L_1 resonances. For the chain of 100 spheres, the supercavity resonance has a Q factor of 6.6×10^9 and a giant F_P factor of $> 10^{10}$. Such high F_P and Q values are useful for quantum networks [7], on-chip quantum light sources [9], and on-chip nanolasers [10].

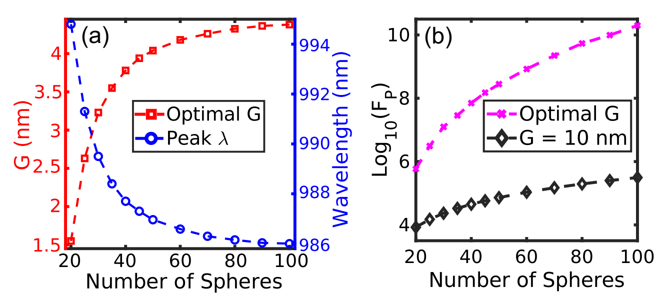

FIG. 4. Dependence of the supercavity L_1 resonance on the number of spheres. (a) The optimal gap and its associated wavelength of the mode converge to $G = 4.5$ nm and $\lambda = 986$ nm, respectively. (b) Purcell factor in logarithmic scale. Two plots associating with the supercavity L_1 resonance (optimal G) and the normal L_1 resonance at $G = 10$ nm are presented for comparison.

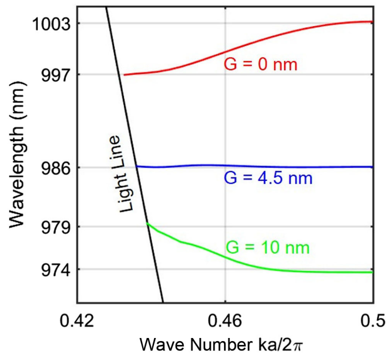

FIG. 5. Band structures for three different gap sizes indicate that the flatband occurs at $G = 4.5$ nm.

Figure 5 displays the band structure of the quasi-1D PC for three different gap sizes obtained from a numerical solution of Maxwell's equations [10]. Intriguingly, these PC bands can also be derived from a multipole expansion approach concerning the Bloch waves supported by infinite arrays of high-index spheres, where the long-range coupling is accounted for [25]. However, we note that Bloch waves fall short in comprehensively representing both propagating and standing waves within finite arrays of spheres [37]. All three bands in Fig. 5 are situated below the light line, which characterizes them as guided PC modes. A remarkably flat band appears at $\lambda = 986$ nm for $G = 4.5$ nm, or equivalently $a = 424.5$ nm. The other two bands, with $G = 0$ nm and $G = 10$ nm, have bandwidths of 6 and 5 nm, respectively. The positions of the two band edge L_1 modes for $G = 0$ nm and $G = 10$ nm, relative to their bands, reflect the crossing of the collective Mie resonances, as presented in Fig. 2(c). This confirms that the origin of the Bloch flatband at $\lambda = 986$ nm is due to the degeneracy of the collective resonances. In the PC context, since the flatband is situated below the light line, its origin is the degeneracy of a continuum of guided PC modes achieved via fine-tuning. While conventional wisdom expects the Bloch flatband to decouple from the far-field region, here the flatband forms a resonance with a large but finite Q factor. This phenomenon is similar to photonic flatband resonances above the light line, as discussed in [11]. Therefore, the multiple scattering theory provides a powerful framework for probing flatband physics from both PC and scattering perspectives.

Conclusions.—We have elucidated the origin of the flatband resonances in the multiple multipole Mie scattering, and have demonstrated that they arise from a degeneracy of the collective resonances. Hybridizing the flatband resonance with an electric hot spot mode can lead to a giant enhancement of the Purcell factor of an electric dipolar emitter. Our findings not only shed light on the physics of other flatband systems, including those based on moiré structures [16,56], but also suggest a smart optimization of nanophotonic quantum devices. Our multiple multipole scattering approach is applicable to cavities of arbitrary shapes, and it offers a powerful semianalytical approach for the study of the quantum interaction between nanostructures and multipolar emitters [57]. Each multipole mode can also serve as a quasinormal mode for the second quantization of the electromagnetic field in a nanophotonic system [44–46,58,59], providing a node in a quantum network [60].

This research is supported by Agency for Science, Technology and Research (A*STAR) under its Career Development Fund (C210112012). T. X. H thanks H.-S. Chu, F. J. García-Vidal, and C. E. Png for helpful discussions. D. L. acknowledges support from the National Research Foundation, Singapore and A*STAR under its CQT Bridging Grant. Y. K. acknowledges support from the Australian Research Council (Grant No. DP210101292).

[1] B. Sutherland, Localization of electronic wave functions due to local topology, Phys. Rev. B **34**, 5208 (1986).
[2] D. Leykam, A. Andreanov, and S. Flach, Artificial flat band systems: From lattice models to experiments, Adv. Phys. **3**, 1473052 (2018).
[3] E. J. Bergholtz and Z. Liu, Topological flat band models and fractional Chern insulators, Int. J. Mod. Phys. B **27**, 1330017 (2013).
[4] L. Balents, C. R. Dean, D. K. Efetov, and A. F. Young, Superconductivity and strong correlations in moiré flat bands, Nat. Phys. **16**, 725 (2020).
[5] D. Leykam and S. Flach, Perspective: Photonic flatbands, APL Photonics **3**, 070901 (2018).
[6] L. Tang, D. Song, S. Xia, S. Xia, J. Ma, W. Yan, Y. Hu, J. Xu, D. Leykam, and Z. Chen, Photonic flat-band lattices and unconventional light localization, Nanophotonics **9**, 1161 (2020).
[7] A. Reiserer and G. Rempe, Cavity-based quantum networks with single atoms and optical photons, Rev. Mod. Phys. **87**, 1379 (2015).
[8] D. B. Higginbottom *et al.*, Optical observation of single spins in silicon, Nature (London) **607**, 266 (2022).
[9] F. Liu, A. J. Brash, J. O'Hara, L. M. P. P. Martins, C. L. Phillips, R. J. Coles, B. Royall, E. Clarke, C. Bentham, N. Prtljaga, I. E. Itskevich, L. R. Wilson, M. S. Skolnick, and A. M. Fox, High Purcell factor generation of indistinguishable on-chip single photons, Nat. Nanotechnol. **13**, 835 (2018).
[10] T. X. Hoang, S. T. Ha, Z. Pan, W. K. Phua, R. Paniagua-Domínguez, C. E. Png, H.-S. Chu, and A. I. Kuznetsov, Collective Mie resonances for directional on-chip nanolasers, Nano Lett. **20**, 5655 (2020).
[11] Y. Yang, C. Roques-Carmes, S. E. Kooi, H. Tang, J. Beroz, E. Mazur, I. Kaminer, J. D. Joannopoulos, and M. Soljačić, Photonic flatband resonances for free-electron radiation, Nature (London) **613**, 42 (2023).
[12] R. A. Vicencio Poblete, Photonic flat band dynamics, Adv. Phys. **6**, 1878057 (2021).
[13] H. S. Nguyen, F. Dubois, T. Deschamps, S. Cueff, A. Pardon, J.-L. Leclercq, C. Seassal, X. Letartre, and

P. Viktorovitch, Symmetry breaking in photonic crystals: On-demand dispersion from flatband to Dirac cones, Phys. Rev. Lett. **120**, 066102 (2018).

[14] J. M. B. Lopes dos Santos, N. M. R. Peres, and A. H. Castro Neto, Graphene bilayer with a twist: Electronic structure, Phys. Rev. Lett. **99**, 256802 (2007).

[15] R. Bistritzer and A. H. MacDonald, Moiré bands in twisted double-layer graphene, Proc. Natl. Acad. Sci. U.S.A. **108**, 12233 (2011).

[16] P. Wang, Y. Zheng, X. Chen, C. Huang, Y. V. Kartashov, L. Torner, V. V. Konotop, and F. Ye, Localization and delocalization of light in photonic moiré lattices, Nature (London) **577**, 42 (2020).

[17] H. Tang, F. Du, S. Carr, C. DeVault, O. Mello, and E. Mazur, Modeling the optical properties of twisted bilayer photonic crystals, Light Sci. Appl. **10**, 157 (2021).

[18] K. Dong, T. Zhang, J. Li, Q. Wang, F. Yang, Y. Rho, D. Wang, C. P. Grigoropoulos, J. Wu, and J. Yao, Flat bands in magic-angle bilayer photonic crystals at small twists, Phys. Rev. Lett. **126**, 223601 (2021).

[19] B. Lou, N. Zhao, M. Minkov, C. Guo, M. Orenstein, and S. Fan, Theory for twisted bilayer photonic crystal slabs, Phys. Rev. Lett. **126**, 136101 (2021).

[20] L. Huang, W. Zhang, and X. Zhang, Moiré quasibound states in the continuum, Phys. Rev. Lett. **128**, 253901 (2022).

[21] D. X. Nguyen, X. Letartre, E. Drouard, P. Viktorovitch, H. C. Nguyen, and H. S. Nguyen, Magic configurations in moiré superlattice of bilayer photonic crystals: Almost-perfect flatbands and unconventional localization, Phys. Rev. Res. **4**, L032031 (2022).

[22] H. C. Po, L. Zou, T. Senthil, and A. Vishwanath, Faithful tight-binding models and fragile topology of magic-angle bilayer graphene, Phys. Rev. B **99**, 195455 (2019).

[23] S. Carr, S. Fang, H. C. Po, A. Vishwanath, and E. Kaxiras, Derivation of Wannier orbitals and minimal-basis tight-binding Hamiltonians for twisted bilayer graphene: First-principles approach, Phys. Rev. Res. **1**, 033072 (2019).

[24] X. Huang, Y. Lai, Z. H. Hang, H. Zheng, and C. T. Chan, Dirac cones induced by accidental degeneracy in photonic crystals and zero-refractive-index materials, Nat. Mater. **10**, 582 (2011).

[25] C. Linton, V. Zalipaev, and I. Thompson, Electromagnetic guided waves on linear arrays of spheres, Wave Motion **50**, 29 (2013).

[26] W. Liu and Y. S. Kivshar, Multipolar interference effects in nanophotonics, Phil. Trans. R. Soc. A **375**, 20160317 (2017).

[27] S. Gladyshev, A. Shalev, K. Frizyuk, K. Ladutenko, and A. Bogdanov, Bound states in the continuum in multipolar lattices, Phys. Rev. B **105**, L241301 (2022).

[28] A. Lagendijk and B. A. van Tiggelen, Resonant multiple scattering of light, Phys. Rep. **270**, 143 (1996).

[29] T. X. Hoang, S. N. Nagelberg, M. Kolle, and G. Barbastathis, Fano resonances from coupled whispering-gallery modes in photonic molecules, Opt. Express **25**, 13125 (2017).

[30] C. E. Whittaker, E. Cancellieri, P. M. Walker, D. R. Gulevich, H. Schomerus, D. Vaitiekus, B. Royall, D. M. Whittaker, E. Clarke, I. V. Iorsh, I. A. Shelykh, M. S. Skolnick, and D. N. Krizhanovskii, Exciton polaritons in a two-dimensional Lieb lattice with spin-orbit coupling, Phys. Rev. Lett. **120**, 097401 (2018).

[31] M. Milićević, G. Montambaux, T. Ozawa, O. Jamadi, B. Real, I. Sagnes, A. Lemaître, L. Le Gratiet, A. Harouri, J. Bloch, and A. Amo, Type-III and tilted Dirac cones emerging from flat bands in photonic orbital graphene, Phys. Rev. X **9**, 031010 (2019).

[32] G. Cáceres-Aravena, D. Guzmán-Silva, I. Salinas, and R. A. Vicencio, Controlled transport based on multiorbital Aharonov-Bohm photonic caging, Phys. Rev. Lett. **128**, 256602 (2022).

[33] T. X. Hoang, X. Chen, and C. J. R. Sheppard, Multipole and plane wave expansions of diverging and converging fields, Opt. Express **22**, 8949 (2014).

[34] T. Liu, R. Xu, P. Yu, Z. Wang, and J. Takahara, Multipole and multimode engineering in Mie resonance-based metastructures, Nanophotonics **9**, 1115 (2020).

[35] T. X. Hoang, H.-S. Chu, F. J. García-Vidal, and C. E. Png, High-performance dielectric nano-cavities for near- and mid-infrared frequency applications, J. Opt. **24**, 094006 (2022).

[36] J. D. Jackson, *Classical Electrodynamics* (John Wiley & Sons, New York, 1999).

[37] See Supplemental Material at http://link.aps.org/supplemental/10.1103/PhysRevLett.132.043803, which contains further analysis of the collective modes.

[38] A. Devaney and E. Wolf, Multipole expansions and plane wave representations of the electromagnetic field, J. Math. Phys. (N.Y.) **15**, 234 (1974).

[39] W. Chew and Y. Wang, Efficient ways to compute the vector addition theorem, J. Electromagn. Waves Appl. **7**, 651 (1993).

[40] M. S. Sidorenko, O. N. Sergaeva, Z. F. Sadrieva, C. Roques-Carmes, P. S. Muraev, D. N. Maksimov, and A. A. Bogdanov, Observation of an accidental bound state in the continuum in a chain of dielectric disks, Phys. Rev. Appl. **15**, 034041 (2021).

[41] D. F. Kornovan, R. S. Savelev, Y. Kivshar, and M. I. Petrov, High-Q localized states in finite arrays of subwavelength resonators, ACS Photonics **8**, 3627 (2021).

[42] R. M. Bakker, Y. F. Yu, R. Paniagua-Domínguez, B. Luk'yanchuk, and A. I. Kuznetsov, Resonant light guiding along a chain of silicon nanoparticles, Nano Lett. **17**, 3458 (2017).

[43] E. N. Bulgakov and A. F. Sadreev, High-Q resonant modes in a finite array of dielectric particles, Phys. Rev. A **99**, 033851 (2019).

[44] C. Sauvan, J. P. Hugonin, I. S. Maksymov, and P. Lalanne, Theory of the spontaneous optical emission of nanosize photonic and plasmon resonators, Phys. Rev. Lett. **110**, 237401 (2013).

[45] P. T. Kristensen and S. Hughes, Modes and mode volumes of leaky optical cavities and plasmonic nanoresonators, ACS Photonics **1**, 2 (2014).

[46] S. Franke, S. Hughes, M. K. Dezfouli, P. T. Kristensen, K. Busch, A. Knorr, and M. Richter, Quantization of quasinormal modes for open cavities and plasmonic cavity quantum electrodynamics, Phys. Rev. Lett. **122**, 213901 (2019).

[47] H. Friedrich and D. Wintgen, Interfering resonances and bound states in the continuum, Phys. Rev. A **32**, 3231 (1985).

[48] C. W. Hsu, B. Zhen, A. D. Stone, J. D. Joannopoulos, and M. Soljačić, Bound states in the continuum, Nat. Rev. Mater. **1**, 16048 (2016).

[49] M. V. Rybin, K. L. Koshelev, Z. F. Sadrieva, K. B. Samusev, A. A. Bogdanov, M. F. Limonov, and Y. S. Kivshar, High-Q supercavity modes in subwavelength dielectric resonators, Phys. Rev. Lett. **119**, 243901 (2017).

[50] T. X. Hoang, X. Chen, and C. J. R. Sheppard, Interpretation of the scattering mechanism for particles in a focused beam, Phys. Rev. A **86**, 033817 (2012).

[51] L. Fonda, Bound states embedded in the continuum and the formal theory of scattering, Ann. Phys. (N.Y.) **22**, 123 (1963).

[52] J. D. Joannopoulos, S. G. Johnson, J. N. Winn, and R. D. Meade, *Photonic Crystals: Molding the Flow of Light* (Princeton University Press, Princeton, NJ, 2008).

[53] S. G. Johnson, S. Fan, P. R. Villeneuve, J. D. Joannopoulos, and L. A. Kolodziejski, Guided modes in photonic crystal slabs, Phys. Rev. B **60**, 5751 (1999).

[54] S. Fan and J. D. Joannopoulos, Analysis of guided resonances in photonic crystal slabs, Phys. Rev. B **65**, 235112 (2002).

[55] Z. Sadrieva, K. Frizyuk, M. Petrov, Y. Kivshar, and A. Bogdanov, Multipolar origin of bound states in the continuum, Phys. Rev. B **100**, 115303 (2019).

[56] X.-R. Mao, Z.-K. Shao, H.-Y. Luan, S.-L. Wang, and R.-M. Ma, Magic-angle lasers in nanostructured moiré superlattice, Nat. Nanotechnol. **16**, 1099 (2021).

[57] L. Novotny and B. Hecht, *Principles of Nano-Optics* (Cambridge University Press, Cambridge, England, 2006).

[58] P. Lodahl, S. Mahmoodian, and S. Stobbe, Interfacing single photons and single quantum dots with photonic nanostructures, Rev. Mod. Phys. **87**, 347 (2015).

[59] I. Medina, F. J. García-Vidal, A. I. Fernández-Domínguez, and J. Feist, Few-mode field quantization of arbitrary electromagnetic spectral densities, Phys. Rev. Lett. **126**, 093601 (2021).

[60] C. Fabre and N. Treps, Modes and states in quantum optics, Rev. Mod. Phys. **92**, 035005 (2020).